PCCP

RSC Publishing

PAPER

View Article Online
View Journal | View Issue

Cite this: *Phys. Chem. Chem. Phys.*, 2013, **15**, 18702

Charged stacks of dithiin, diselenin, thianthrene and selenanthrene radical cations: long range multicenter bonds

Michael F. Peintinger,*[a] Johannes Beck[b] and Thomas Bredow[a]

Received 10th August 2013,
Accepted 17th September 2013

DOI: 10.1039/c3cp53410c

www.rsc.org/pccp

The bonding mechanism of charged stacks of thianthrene and selenanthrene radical cations is studied using quantum-chemical methods. The investigation of the nature of the electronic ground state and the electronic structure *via* gas-phase multireference calculations brings insight into the interactions of such dimers and trimers as found in molecular crystals. Since thianthrene and selenanthrene are the dibenzo-homologues of dithiin and diselenin, the latter are taken as model systems to study the influence of the ring systems. For all investigated systems, the singlet state is the ground state. Multicenter bonds are formed between the singular occupied orbitals of the radicals. All dimers are found to be metastable. The thianthrene trimers, which are experimentally found in molecular crystals are also stable in the gas phase, while the analogue selenanthrene trimers are not.

1 Introduction

Organic semiconducting materials are in the focus of intensive research due to their electronic properties, mechanic flexibility and the vast possibilities for chemical modifications.[1] Applications in electronic and optoelectronic devices are organic light-emitting diodes,[2] field-effect transistors[3,4] and solar cells.[5] If such systems feature unpaired electrons in ground or electronically excited states, they have the potential for high and complex reactivity and the emergence of magnetic properties. Such spin centers in semiconductors made up of organic radical cations may lead to materials exhibiting magnetic properties besides the conductivity and find applications in spintronics.[6] If the organic radicals are of planar shape, stacked arrangements of these cations can occur, thus leading to interactions of these spin centers. Understanding the interactions of these spin centers is crucial for the design of novel multi-functional materials.[7,8]

The reaction of thianthrene (TA) with the thianthrene radical cation ($TA^{+\bullet}$) has been known for over a hundred years.[9–12] The reversible formation of TA radical dimers was confirmed by *in situ* ESR/UV-Vis-NIR spectroelectrochemical experiments.[13] While selenanthrene (SeA) is generally less explored than thianthrene, it is known that it undergoes a one-electron oxidation to form the radical cation and a second oxidation step to form the dication.[14,15]

In a previous study we reported the synthesis of TA[PF6] that features $TA^{+\bullet}$ dimers in local C_{2h} point group symmetry, slightly distorted from perfect D_{2h} symmetry. Periodic calculations of the relative stability in the singlet and triplet state gave contradicting results, depending on the method. While the Hartree–Fock method predicts the triplet state to be more stable by 0.4 eV, the PBE functional[16] favors the singlet state by 1.0 eV and the hybrid approaches PBE0[17] and PW1PW[18] predicted the singlet state to be 0.7 eV more stable than the triplet state.

Rosokha *et al.* synthesized $[TA_3^{2+}]\cdot 2(C_{13}H_{36}B_{11})^{-}\cdot 4CH_2Cl_2$ where the TA radicals form a crossed triple-decker dication.[19] In a recent publication we reported on the reactions of TA and SeA with $AlCl_3$. The solvent-free reaction of TA with $AlCl_3$ yielded $TA_3[Al_2Cl_7]_2$ which features parallel stacked trimers of TA.[20] The corresponding reaction of selenanthrene (SeA) yielded $[Al(SeA)_3][Al_2Cl_7]_3$, where the tris–chelate complex ion $[Al(SeA)_3]^{3+}$ with SeA acting as a bidentate ligand and both Se atoms binding to the octahedrally coordinated Al^{3+} ion was formed. No SeA-trimers were found. With SO_2 as solvent, both TA and SeA give radical salts $(TA)_2[AlCl_4]_2$ and $(SeA)_2[AlCl_4]_2$, respectively. Both systems consist of dimers of TA^+ (SeA^+) radical ions, which are bound by weak intermolecular forces. In that study we have theoretically studied these crystals with the periodic HF-DFT hybrid method employing the PW1PW[18] functional and pob-TZVP basis sets[21] as well as with molecular calculations with the PBE0 functional[17] and dispersion correction.[22]

Density functional theory takes into account dynamic correlation effects. But an accurate quantum-chemical description of the electronic properties of molecular crystals featuring spin centers needs to treat both static and dynamic electron

[a] *Mulliken Center for Theoretical Chemistry, University of Bonn, Beringstr. 4, 53115 Bonn, Germany. E-mail: mpei@thch.unibonn.de; Tel: +49 228 733834*
[b] *Institute for Inorganic Chemistry, University of Bonn, Bonn, Germany*

correlation effects in an accurate way. At present multi-reference methods are not applicable for periodic systems with many atoms in the unit cells. One possibility is the application of multi-reference *ab initio* methods using cluster models that represent a small portion of the molecular crystal. For a deeper understanding of the electronic structure and the bonding mechanism of the dimers and trimers inside the above-mentioned radical salts, we now performed highly-accurate multi-reference calculations on selected fragments of the molecular crystals.

As TA is the dibenzo-homologue of 1,4-dithiin (DT), the latter is an ideal model system to investigate the effect of the benzene rings on the electronic structure and the bonding mechanism of the TA_n dimers and trimers. The same is true for SeA and 1,4-diselenin (DSe) and SeA_n dimers and trimers.

2 Computational details

All molecular as well as free and embedded cluster calculations were carried out using the ORCA program system.[23] For structure optimizations and for the generation of initial natural orbitals (NOs) for our multi-reference calculations the spin-component-scaled variant of Møller–Plesset Perturbation Theory of 2nd order[24] combined with the resolution-of-identity-approximation (SCS-RI-MP2) with relaxed densities was applied. This method has been shown to give better results than MP2 itself.[25,26]

Configuration interaction expansions built on natural orbitals show the fastest possible convergence.[27] Natural orbitals with negligible occupation numbers were omitted from the one-electron space. The multi-configurational complete active space self-consistent field (CASSCF) method[28] was applied to the NOs generated from SCS-RI-MP2 with relaxed densities for the efficient treatment of long-range static correlation.

Strongly-contracted *n*-electron valence perturbation theory of 2nd order (SC-NEVPT2)[29–31] on top of CASSCF allows efficient treatment of short-range dynamic correlation. In contrast to second-order multi-configurational perturbation theory (CASPT2),[32] SC-NEVPT2 does not suffer from the so-called intruder state problem. It is size-consistent and due to internal contraction it is independent of the reference space. Therefore we applied SC-NEVPT2 on top of the CASSCF-wavefunction (CAS(*m*,*n*)-NEVPT2) to include dynamic correlation effects. In this notation the active space consists of *m* electrons and *n* orbitals.

To make the SCS-RI-MP2 and especially the (multi-reference) CAS-NEVPT2 calculations with over a thousand basis functions feasible, while introducing only a small error, the "chain-of-spheres" algorithm for the Hartree–Fock exchange in combination with Split-RI-J for the Coulomb part (RIJCOSX) approximation[33] was employed.

The well-proven Karlsruhe def2-SVP[34,35] and def2-TZVP[36,37] basis sets were employed. All monomers and dimers, as well as the trimer structures of DT and DSe, were optimized employing the TZVP basis sets. For the structure optimizations of the larger trimer structures of TA and SeA, the SVP basis sets were used.

For the selenium containing compounds, structure optimizations were also checked employing the Douglas–Kroll–Hess (DKH) scalar relativistic Hamiltonians.[38] No significant differences were found compared to the non-relativistic calculations.

To account for the problem of the basis set superposition error (BSSE) when calculating the dissociation energies, we estimated the Counterpoise correction (CPC) with the geometrical Counterpoise correction (gCP) scheme at the HF/TZVP level.[39,40] Although this scheme is meant to be used for HF and not for MP2, it should give a crude approximation of the BSSE for MP2.

The effect of the Madelung potential on the singlet–triplet splitting was studied *via* the embedded cluster model employing large grids of point charges.

Figures were generated with Gabedit.[41]

3 Results and discussion

3.1 Neutral molecules and radicals

The neutral DT, DSe, TA and SeA molecules have C_{2v} symmetry and are bent along the intramolecular S–S, respectively, Se–Se axis.[42–45] While in the literature general bending angles α of TA and SeA are given, there are in fact two dihedral angles to take into consideration. The two dihedral angles α_1 (X1–C2–C7–C6) and α_2 (C2–X1–X8–C9) both reflect the bending of the molecule and give it a hat-like structure (see Fig. 1 and 2 for the numbering scheme of atoms).

Vashchenko *et al.*[46] discussed this problem when studying the macrocyclization of DT. In order to compare our calculated angles to the experiment we summed up both dihedral angles α_1 and α_2 to reproduce the general bending angle α. The results given in Table 1 are in good agreement with the experiment. Nevertheless, this is just an approximation and finer resolved experimental data are needed for a more accurate comparison. The bending of the molecules leads to a dipole moment, which was calculated to be 1.3 D for DT, 1.7 D for TA, 1.2 D for DSe and 1.6 D for SeA.

Gallaher and Bauer[48] have studied the structure and inversion potential of TA in the gas-phase. Our calculated structural

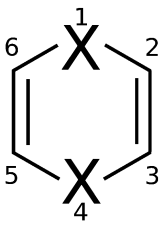

Fig. 1 Numbering scheme of atoms in DT and DSe (X = S, Se).

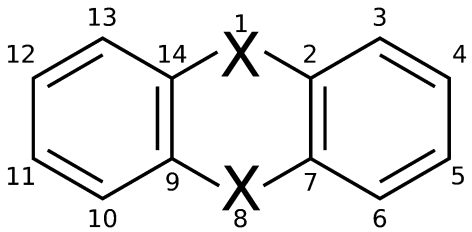

Fig. 2 Numbering scheme of atoms in TA and SeA (X = S, Se).

Table 1 Experimental and calculated (SCS-MP2/TZVP) bending angles of DT, TA, DSe and SeA

Molecule	Exp.	α	α_1	α_2
DT	137 [42]	138.2	2.9	135.3
TA	128 [47]	127.9	2.2	125.7
DSe	—	131.0	3.3	127.7
SeA	127 [45]	125.0	1.5	123.5

parameters are in agreement with their results, except for the intramolecular S–S distance, which they found to be 2.74 Å. Our calculated S–S distance of 3.28 Å differs significantly. We have checked these findings with the a different theoretical model (hybrid-method PBE0[17]) which gives exactly the same result and therefore we gained some confidence that our results are correct.

After oxidation to the radical cation, all molecules undergo a structure change from bent to planar shape. The energy difference of the neutral species between the planar D_{2h} structure and the bent C_{2v} structures, corresponding to the barrier of ring inversion, is 0.30 eV DT, 0.31 eV for TA 0.40 eV for DSe and 0.43 eV for SeA.

For the optimized structures, CASSCF-SC-NEVPT2 calculations were performed on the neutral molecules and the radical cations.

The calculated adiabatic and vertical ionization energies are given in Table 2. They are in excellent agreement with the experiment.[49] The ionization potentials of the dibenzo-homologues are slightly lower than for the model systems, due to a small stabilization effect of the outer benzene ring.

The calculated natural orbitals with occupation numbers of 1.0 (SONO) corresponding to the singly occupied molecular orbitals of $DT^{+\bullet}$ (Fig. 3) and $TA^{+\bullet}$ (Fig. 4) show that the unpaired electron of the radical cations is mainly delocalized over the central hetero-cycle. The congruous NOs of $DSe^{+\bullet}$ and $SeA^{+\bullet}$ have almost identical shape. This supports the idea of using DT and DSe as model systems for TA and SeA.

Table 2 Experimental and calculated ionization potentials (eV) of DT, TA, DSe and SeA in the gas-phase

Compound	Property	Experiment	SCS-RI-MP2	CAS-NEVPT2
DT	IP_v	8.1	8.0	7.9
	IP_a		7.3	7.1
TA	IP_v	7.8	7.9	7.7
	IP_a		7.3	7.0
DSe	IP_v	8.1	8.0	7.9
	IP_a		7.3	7.2
SeA	IP_v	7.9	8.1	7.8
	IP_a		7.3	7.3

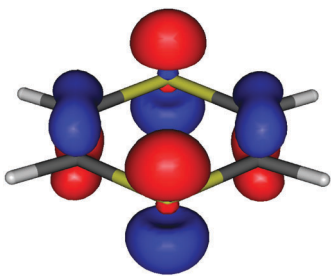

Fig. 3 Calculated (CAS(5,6)-NEVPT2, def2-TZVP) natural orbital with occupation numbers of 1.0 (SONO) corresponding to the singly occupied molecular orbital of $DT^{+\bullet}$. The calculated SONOs of $DSe^{+\bullet}$ are of almost identical shape.

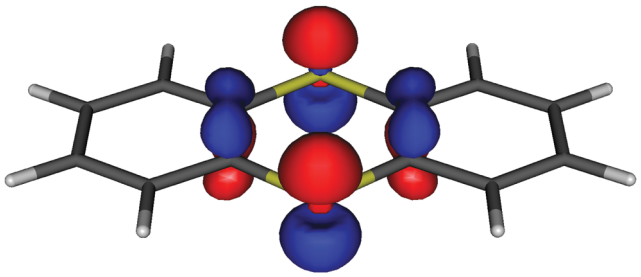

Fig. 4 Calculated (CAS(5,6)-NEVPT2, def2-TZVP) natural orbital with occupation numbers of 1.0 (SONO) corresponding to the singly occupied molecular orbital of $TA^{+\bullet}$. The calculated SONOs of $SeA^{+\bullet}$ are of almost identical shape.

3.2 Radical dimers

The parallel dimers $DT_{2,p}^{2+}$ and $DSe_{2,p}^{2+}$ were optimized in D_{2h} symmetry. $TA_{2,p}^{2+}$ and $SeA_{2,p}^{2+}$ were optimized in symmetrized D_{2h} and the slightly distorted C_i structure, as found experimentally in (TA)PF6 and (SeA)AlCl4.[20,50] If one of the molecules is rotated by 90° around the intermolecular main axis, we refer to these structures as crossed dimers.

In all charged dimers of the investigated radicals, intermolecular 2-electron-4-center (2e4c) bonds are formed between the two natural orbitals with an occupation number of 1.0 of two monomers as can be seen in Fig. 5–7. We will refer to natural orbitals with occupation numbers of 1.0 as singly occupied natural orbitals (SONOs). And we will refer to the natural orbitals closely resembling the highest occupied (lowest unoccupied) molecular orbitals as HONOs (LUNOs), even though their occupation numbers differ from 2.0 and 0.0.

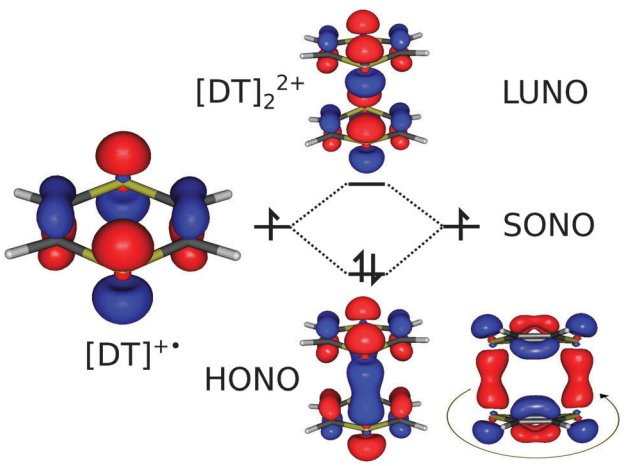

Fig. 5 NO diagram arising from coupling of the two SONOs (NO with occupation number of 1.0) on each $DT^{+\bullet}$ forming DT_2 bonding and antibonding orbitals. Occupation numbers are 1.4 for the HONO and 0.6 for the LUNO.

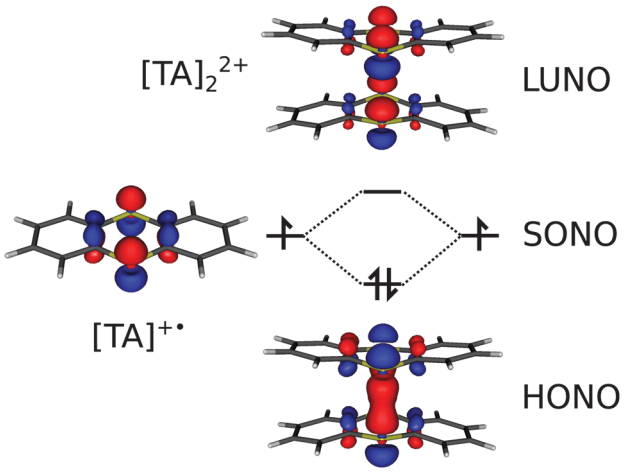

Fig. 6 NO diagram arising from coupling of the two SONOs (NO with occupation number of 1.0) on each $TA^{+\bullet}$ forming TA_2^{2+} (parallel) bonding and antibonding orbitals. Occupation numbers are 1.4 for the HONO and 0.6 for the LUNO.

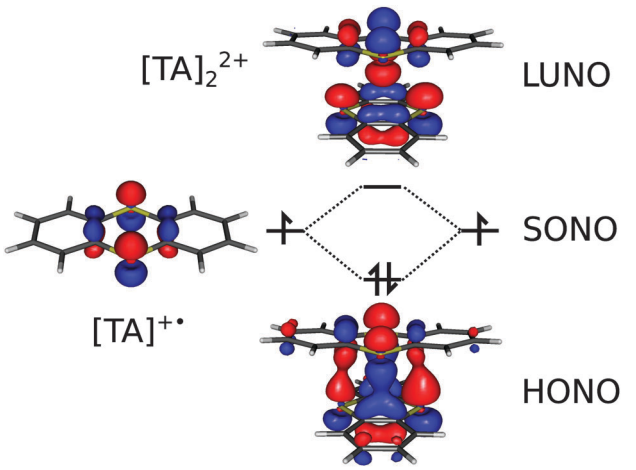

Fig. 7 NO diagram arising from coupling of the two SONOs (NO with occupation number of 1.0) on each $TA^{+\bullet}$ forming TA_2^{2+} (crossed) bonding and antibonding orbitals. Occupation numbers are 1.4 for the HONO and 0.6 for the LUNO.

We calculated the dissociation E_d energy for all charged dimers according to

$$X_2^{2+} \rightarrow 2X^{+\bullet} \quad (1)$$

All compounds are only meta-stable in the gas-phase as indicated by the negative values of E_d. The BSSE-corrected dissociation energies at the SCS-MP2/TZVP level are given in Table 3. They are lower for the model systems than for the dibenzo-homologues, since the ring systems have a stabilization effect *via* dispersion interactions.

In D_{2h} symmetry, the intermolecular S–S bond in $DT_{2,p}^{2+}$ is 3.04 Å. In $TA_{2,p}^{2+}$ the bond is slightly shortened to 3.00 Å due to dispersion interaction between the two outer benzene rings.

The optimization of $TA_{2,p}^{2+}$ starting in C_i structure also ends up in the D_{2h} structure. As expected, the Se–Se bond distance of

Table 3 Calculated X–X distances D_{X-X} (X = S, Se) and dissociation energies E_d of parallel (''p'') and crossed (''c'') dimers DT_2^{2+}, TA_2^{2+}, DSe_2^{2+} and SeA_2^{2+} at SCS-RI-MP2. ΔE is the difference in total energy of two radical cations and the charged dimers. E_{gCP} is the counterpoise correction energy. Lengths are given in Å and energies are given in eV

	Basis set				
	SVP	TZVP			
Compound	D_{X-X}	D_{X-X}	ΔE	E_{gCP}	E_d
$DT_{2,p}^{2+}$	3.07	3.04	−2.08	−0.18	−2.25
$DT_{2,c}^{2+}$	3.95	3.95	−2.21	−0.17	−2.39
$TA_{2,p}^{2+}$	2.99	3.00	−0.77	−0.37	−1.14
$TA_{2,c}^{2+}$	3.79	3.79	−0.74	−0.37	−1.12
$DSe_{2,p}^{2+}$	3.25	3.22	−1.84	−0.34	−2.19
$DSe_{2,c}^{2+}$	4.22	4.20	−2.08	−0.35	−2.43
$SeA_{2,p}^{2+}$	3.21	3.20	−0.70	−0.55	−1.25
$SeA_{2,c}^{2+}$	4.05	4.04	−0.74	−0.57	−1.31

the isoelectronic $DSe_{2,p}^{2+}$ (3.22) and $SeA_{2,p}^{2+}$ (3.20 Å) are larger than for the sulfur compounds. The C_i structure of SeA_2^{2+} is almost isoenergetic ($\Delta E_{D_{2h}-C_i}$ = 0.03 eV) with the D_{2h} structure.

The parallel arrangement is favored for all dimers (DT: 0.14 eV, DSe: 0.24 eV, SeA: 0.04 eV), except for TA, where the crossed arrangement is 0.03 eV lower in energy.

For the crossed dimers, the X–X distances are longer, since the heteroatoms are not directly stacked (see Table 3), but the inter-layer distances are shorter, 3.10 Å (DT), 2.88 Å (TA), 3.22 Å (DSe) and 3.10 Å (SeA). The distance between the heteroatom of one molecule and the opposing center of the C–C bond of the other molecule corresponds to an inter-layer distance.

The active space of the CASSCF calculations was selected to include six electrons and six orbitals. The states were averaged over singlet and triplet states. Also 4–4 and 8–8 active spaces were checked and showed no significant differences, since the most relevant orbitals for the excitation are already included in the active space.

For all investigated dimers, the closed-shell singlet state is the ground state. The excitation energy for $DT_{2,p}^{2+}$ to the triplet state is 1.0 eV and 3.0 eV to the next higher singlet state. For $TA_{2,p}^{2+}$ the ground state excitation energy to the triplet state is 1.1 eV. Compared to $DT_{2,p}^{2+}$, the next higher singlet state is stabilized by the two outer benzene rings and lies only 2.0 eV above the closed-shell singlet ground state. The singlet–triplet splitting energies in crossed dimers $DT_{2,c}^{2+}$ (0.8 eV) and $TA_{2,c}^{2+}$ (1.0 eV) are almost identical to those found in the parallel dimers. The singlet–triplet splitting energy obtained from our multi-reference calculations confirms our previously reported results with periodic band structure and gas-phase hybrid DFT calculations.[20,50]

Fig. 5 shows the natural orbital diagram of the charged $DT_{2,p}^{2+}$ dimer. The HONO is formed from the two SONOs of the two $DT^{+\bullet}$ and shows the long range intermolecular 2e4c S–S bonds. In analogy to the NO diagram of our model system DT, Fig. 6 and 7 show the natural orbital diagram of the formation of the HONO of the parallel and the crossed dimer from the two HONOs of the two $TA^{+\bullet}$ radicals.

The splitting energies for the selenium containing analogues are similar to those found in the sulfur containing compounds.

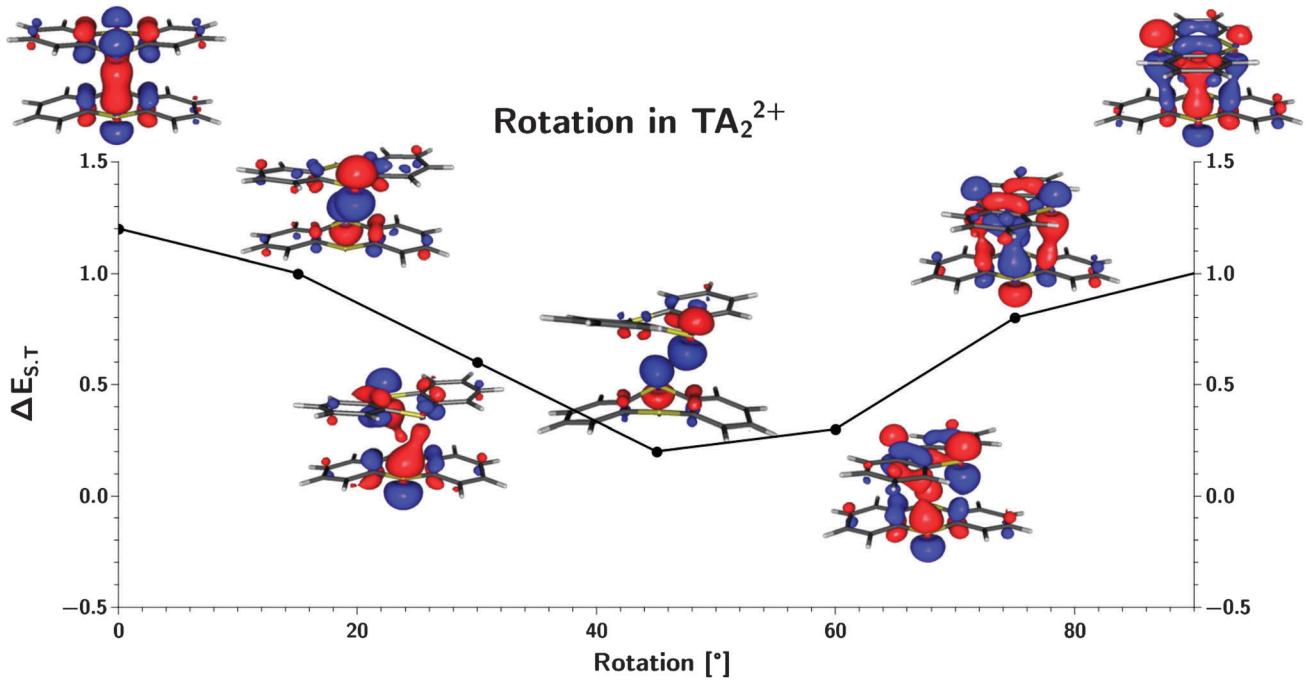

Fig. 8 The figure shows the HONOs and S,T-splitting $E_{S,T}$ depending on the rotation angle of the charged dimer TA_2^{2+}. The rotation angle is given in degrees and energies are given in eV. A positive number indicates that the singlet state is the ground state.

But here we find substantial differences between the parallel and the crossed dimers. For the parallel DSe dimer $DSe_{2,p}^{2+}$ we find a singlet–triplet splitting of 1.1 eV and of 0.9 eV for the parallel SeA dimer $SeA_{2,p}^{2+}$. While in the crossed DSe dimer $DSe_{2,c}^{2+}$ the splitting is lower by 0.4 eV, it is higher by 0.1 eV in the crossed SeA dimer $SeA_{2,c}^{2+}$.

3.3 Rotation of charged dimers

To investigate the dependence of the singlet–triplet splitting on the rotation from the parallel to the crossed dimer, we performed a relaxed scan calculation at the SCS-RI-MP2/def2-TZVP level followed by CAS-NEVPT2 calculations starting from the MP2 natural orbitals. The natural orbitals corresponding to the highest occupied molecular orbitals at different rotation angles are shown in Fig. 8. The singlet–triplet splitting energy $E_{S,T}$ is lowest at 45°, where the singlet and triplet states are almost degenerate and the interaction of the monomers is the weakest. But there is no crossing of the states and therefore the rotation – if it occurs as part of the solid-state reaction – proceeds solely on the singlet hypersurface.

3.4 Radical trimers

For the charged TA trimer (TA_3^{2+}), two different arrangements have been reported. In the parallel trimer $TA_{3,p}^{2+}$ all three TA units are stacked.[20] In the "crossed" trimer $TA_{3,c}^{2+}$, the central TA unit is rotated by 90°.[19] Both structures have been fully optimized at the SCS-RI-MP2-level as charged clusters in the gas-phase. The results are given in Table 4. In general, the intermolecular X–X distance in the parallel trimers is very similar to the interlayer distance in the corresponding crossed trimers.

Table 4 Calculated interlayer distances (ILD, (X–X–X)/2, X = S, Se) and dissociation energy of parallel and crossed trimers of DT_3^{2+}, TA_3^{2+}, DSe_3^{2+} and SeA_3^{2+} at the SCS-RI-MP2-level. Lengths are given in Å and energies are given in eV

	Basis set				
	SVP	TZVP			
Compound	ILD	ILD	ΔE	E_{gCP}	E_d
$DT_{3,p}^{2+}$	3.25	3.26	−0.79	−0.26	−1.05
$DT_{3,c}^{2+}$	3.27	3.28	−0.88	−0.26	−1.14
$TA_{3,p}^{2+}$	3.08	3.12	+0.67	−0.56	+0.11
$TA_{3,c}^{2+}$	3.00	3.04	+0.81	−0.56	+0.25
$DSe_{3,p}^{2+}$	3.44	3.43	−0.61	−0.51	−1.12
$DSe_{3,c}^{2+}$	3.47	3.47	−0.87	−0.52	−1.39
$SeA_{3,p}^{2+}$	3.32	3.31	+0.67	−0.84	−0.17
$SeA_{3,c}^{2+}$	3.27	3.26	+0.77	−0.88	−0.11

They are shorter for the dibenzo-homologues than for DT and DSe due to dispersion interactions of the ring systems.

We calculated the BSSE-corrected dissociation energy E_d for all charged trimers according to

$$X_3^{2+} \rightarrow X + 2X^{+\bullet}. \quad (2)$$

The only stable compounds are $TA_{3,p}^{2+}$ and $TA_{3,c}^{2+}$. All other compounds are meta-stable. This is supported by the fact that for the reaction of TA and SeA with $AlCl_3$ only trimers of TA and no trimers of SeA were found.

While $DT_{3,p}^{2+}$ is 0.09 eV more stable than $DT_{3,c}^{2+}$ and $DSe_{3,p}^{2+}$ is 0.27 eV more stable than $DT_{3,c}^{2+}$, this is the opposite for TA_3^{2+} and SeA_3^{2+}, where the crossed structure is favored by 0.14 eV for TA and 0.06 eV for SeA.

The calculated gas-phase structures of the parallel and crossed TA_3^{2+} are similar to the structure found experimentally

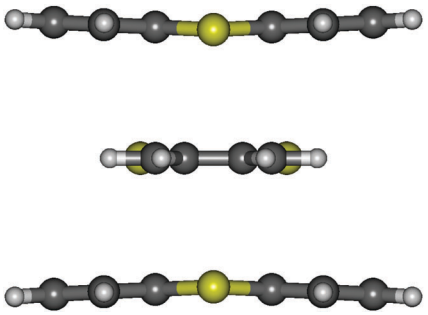

Fig. 9 Optimized structure of $TA_{3,c}^{2+}$ at the SCS-MP2/TZVP level.

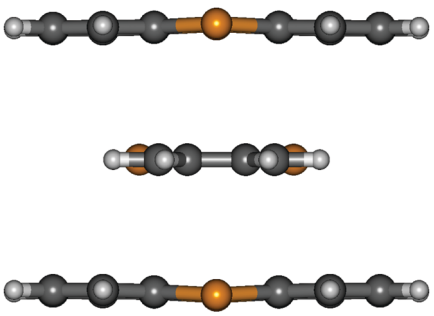

Fig. 10 Optimized structure of $SeA_{3,c}^{2+}$ at the SCS-MP2/TZVP level.

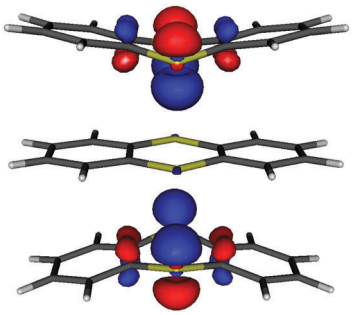

Fig. 11 Natural orbitals corresponding to the highest occupied molecular orbitals of $TA_{3,p}^{2+}$.

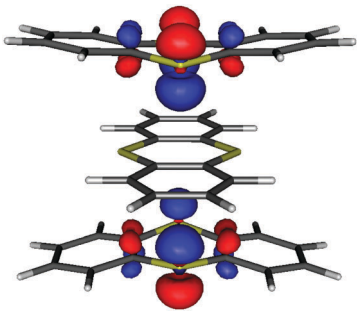

Fig. 12 Natural orbitals corresponding to the highest occupied molecular orbitals of $TA_{3,c}^{2+}$.

in the solid state. Since there are neither crossed nor parallel charged trimers of SeA reported in the literature, we used the optimized TA_3^{2+} structures as a starting structures to optimize SeA_3^{2+}.

While the $SeA_{3,p}^{2+}$ structure is similar to the $TA_{3,p}^{2+}$ with a planar molecule in the center and the two outer molecules bent outwards, the optimized $SeA_{3,c}^{2+}$ structure differs significantly from the one found for the $TA_{3,c}^{2+}$. While in crossed $TA_{3,c}^{2+}$ the outer two TA units are bent outwards (Fig. 9), the opposite is the case in crossed SeA_3^{2+}, where the outer SeA units are slightly bent inwards (Fig. 10).

Here we compare the TA_3^{2+} results to the results of the simpler case of the charged Dithiin trimer DT_3^{2+}. Due to the (with respect to trimers of TA and SeA) missing dispersion interactions of the two benzene rings the distances are larger than in TA_3^{2+}. The intermolecular S$\cdots$S distance of the top and center unit is 3.25 Å in the parallel and 4.10 Å in the crossed trimer. The interlayer distance of the crossed trimer is 3.22 Å. As expected, the intermolecular Se–Se distance in the parallel (3.31 Å) and crossed (4.16 Å) charged selenanthrene trimer is larger than the S–S distances in TA_3^{2+}. The Se–Se distance of the two outer molecules is 6.51 Å, corresponding to an interlayer distance of 3.25 Å.

The singlet–triplet splitting energy of $DT_{3,p}^{2+}$ is much smaller than for the dimer (0.4 eV) and in $DT_{3,c}^{2+}$ it is only 0.2 eV.

The second singlet state is 1.5 eV (1.4 eV) higher in energy in $DT_{3,p}^{2+}$ ($DT_{3,c}^{2+}$) than the ground state.

The singlet–triplet splitting is 0.6 eV in $TA_{3,p}^{2+}$ and only 0.4 eV in $TA_{3,c}^{2+}$. The next singlet is 1.1 eV higher in energy for the parallel and 0.4 eV higher in energy for the crossed trimer.

Due to this small energy difference triplet states may be thermally populated for the structures with crossed trimers of Rosokha *et al.*[19] (Fig. 11 and 12). If the central TA unit of $TA_{3,c}^{2+}$ is removed, the remaining outer TA units are almost non-interacting and singlet and triplet states become degenerate.

For the selenanthrene trimers we find a slightly larger singlet–triplet splitting, 0.7 eV for $SeA_{3,p}^{2+}$ and 0.5 $SeA_{3,c}^{2+}$.

3.5 Effect of the Madelung potential on the singlet–triplet splitting

To test the effect of the Madelung potential on the singlet–triplet splitting we embedded $TA_{3,p}^{2+}$ into a field of point charges. The point charges were derived from the crystal structure of $TA_3Al_2Cl_7$ and were created from 2 × 2 × 2, 5 × 5 × 3 and 7 × 7 × 5 supercells of the conventional unit cell. The point charge values were set up as formal atomic charges, *e.g.* −1 for chlorine and +3 for aluminum. For the molecular cation sulfur was set up as $+\frac{1}{3}$ while carbon and hydrogen were considered neutral. The sum over all charges is zero and no

Table 5 Dependency of the singlet–triplet-splitting of $TA_{3,p}^{2+}$ on the Madelung potential in $TA_3Al_2Cl_7$. *XaYbZc* are point charges of a $X \times \vec{a}$, $Y \times \vec{b}$ and $Z \times \vec{c}$ conventional unit cell with a total number of point charges PCSC. Energies are given in eV

Method	PCSC	Charges	ΔE(S,T)
CAS(6,6)-NEVPT2	2a2b2c	378	0.413
	5a5b3c	28 794	0.628
	7a7b5c	94 074	0.629

overall dipole momentum was introduced. $E_{S,T}$ converges to 0.001 eV with respect to the number of point charges with the $5 \times 5 \times 3$ supercell. The influence of the Madelung potential is found to be negligible (see Table 5), since it does not change the ordering of the electronic states nor give a significant difference for $E_{S,T}$ compared to non-embedded calculations.

4 Conclusion

We investigated the electronic structure of charged stacked arrangements of thianthrene and selenanthrene radical cations as experimentally found in molecular crystals. For all investigated systems, the singlet state is the ground state. In the singlet ground state, the bonding of the dimers is due to formation of σ-bonds between the sulfur (selenium) atoms by combination of the singly occupied orbitals of the monomers. All dimers are found to be metastable in the gas-phase. The ring systems stabilize the dimers significantly.

The bonds of the trimers form essentially due to the overlap of sulfur (selenium) orbitals of the outer rings. The thianthrene trimers, which are experimentally found in molecular crystals, are also stable in the gas phase, while the analogue selenanthrene trimers are not. This is supported by the experiment, where the reaction of SeA with $AlCl_3$ does not tend to form selenanthrene trimers.

The higher stability of the trimers compared to the dimers might be due to the reduced electrostatic repulsion between the radical cations. Thus we conclude that the dimers of TA and SeA found in the radical salts are stabilized by crystal field effects.

Acknowledgements

This material is based on work supported by the German Research Foundation ''Deutsche Forschungsgemeinschaft'' (DFG) within the Collaborative Research Area SFB 813 ''Chemistry at Spin Centers - Concepts, Mechanisms, Functions'' in the Project C5 ''Spin centers in molecular solids - from paramagnetic salts to organic conductors''.

References

1 W. Brütting, *Introduction to the Physics of Organic Semiconductors*, Wiley-VCH Verlag GmbH & Co. KGaA, Weinheim, 2006.
2 R. H. Friend, R. W. Gymer, A. B. Holmes, J. H. Burroughes, R. N. Marks, C. Taliani, D. D. C. Bradley, D. A. D. Santos, J. L. Bredas, M. Logdland and W. R. Salaneck, *Nature*, 1999, **397**, 121–128.
3 W. Clemens, W. Fix, J. Ficker, A. Knobloch and A. Ullmann, *J. Mater. Res.*, 2004, **19**, 1963.
4 G. Horowitz, *J. Mater. Res.*, 2004, **19**, 1946–1962.
5 A. Kahn, N. Koch and W. Gao, *J. Polym. Sci., Part B: Polym. Phys.*, 2003, **41**, 2529–2548.
6 A. R. Rocha, V. M. Garcia-Suarez, S. W. Bailey, C. J. Lambert, J. Ferrer and S. Sanvito, *Nat. Mater.*, 2005, **4**, 335–339.
7 T. Sugawara, H. Komatsu and K. Suzuki, *Chem. Soc. Rev.*, 2011, **40**, 3105–3118.
8 I. Ratera and J. Veciana, *Chem. Soc. Rev.*, 2012, **41**, 303–349.
9 J. Stenhouse, *Proc. R. Soc. London*, 1868, **17**, 62–67.
10 E. Lucken, *J. Chem. Soc.*, 1962, 4963–4965.
11 W. Rundel and K. Scheffler, *Tetrahedron Lett.*, 1963, **4**, 993–995.
12 H. Shine, *Inorg. Nucl. Chem. Lett.*, 1968, **4**, 573.
13 P. Rapta, L. Kress, P. Hapiot and L. Dunsch, *Phys. Chem. Chem. Phys.*, 2002, **4**, 4181–4185.
14 K. Stender, G. Klar and D. Knittel, *Z. Naturforsch., B: Anorg. Chem. Org. Chem.*, 1985, **40**, 774–781.
15 R. Müller, L. Lamberts and M. Evers, *Electrochim. Acta*, 1994, **39**, 2507–2516.
16 J. P. Perdew, K. Burke and M. Ernzerhof, *Phys. Rev. Lett.*, 1996, **77**, 3865–3868.
17 C. Adamo and V. Barone, *J. Chem. Phys.*, 1999, **110**, 6158–6170.
18 T. Bredow and A. R. Gerson, *Phys. Rev. B: Condens. Matter Mater. Phys.*, 2000, **61**, 5194–5201.
19 S. V. Rosokha, J. Lu, T. Y. Rosokha and J. K. Kochi, *Acta Crystallogr., Sect. C: Cryst. Struct. Commun.*, 2007, **63**, 347–349.
20 R. T. Tjahjanto, M. F. Peintinger, T. Bredow and J. Beck, *Eur. J. Inorg. Chem.*, 2012, 3625–3635.
21 M. F. Peintinger, D. V. Oliveira and T. Bredow, *J. Comput. Chem.*, 2013, **34**, 451–459.
22 S. Grimme, J. Antony, S. Ehrlich and H. Krieg, *J. Chem. Phys.*, 2010, **132**, 154104.
23 F. Neese, *Wiley Interdiscip. Rev.: Comput. Mol. Sci.*, 2011, 73–78, DOI: 10.1002/wcms.81.
24 S. Grimme, *J. Chem. Phys.*, 2003, **118**, 9095.
25 S. Grimme, L. Goerigk and R. F. Fink, *Wiley Interdiscip. Rev.: Comput. Mol. Sci.*, 2012, **2**, 886–906.
26 F. Neese, T. Schwabe, S. Kossmann, B. Schirmer and S. Grimme, *J. Chem. Theory Comput.*, 2009, **5**, 3060–3073.
27 E. R. Davidson, *Rev. Mod. Phys.*, 1972, **44**, 451–464.
28 B. O. Roos, P. R. Taylor and P. E. Siegbahn, *Chem. Phys.*, 1980, **48**, 157–173.
29 C. Angeli, R. Cimiraglia and J.-P. Malrieu, *Chem. Phys. Lett.*, 2001, **350**, 297–305.
30 C. Angeli, R. Cimiraglia, S. Evangelisti, T. Leininger and J.-P. Malrieu, *J. Chem. Phys.*, 2001, **114**, 10252–10264.
31 C. Angeli, R. Cimiraglia and J.-P. Malrieu, *J. Chem. Phys.*, 2002, **117**, 9138–9153.
32 K. Andersson, P. A. Malmqvist, B. O. Roos, A. J. Sadlej and K. Wolinski, *J. Phys. Chem.*, 1990, **94**, 5483–5488.
33 F. Neese, F. Wennmohs, A. Hansen and U. Becker, *Chem. Phys.*, 2009, **356**, 98–109.
34 A. Schäfer, H. Horn and R. Ahlrichs, *J. Chem. Phys.*, 1992, **97**, 2571.
35 A. Schäfer, C. Huber and R. Ahlrichs, *J. Chem. Phys.*, 1994, **100**, 5829.
36 F. Weigend, M. Häser, H. Patzelt and R. Ahlrichs, *Chem. Phys. Lett.*, 1998, **294**, 143–152.
37 F. Weigend and R. Ahlrichs, *Phys. Chem. Chem. Phys.*, 2005, **7**, 3297–3305.
38 D. A. Pantazis, X.-Y. Chen, C. R. Landis and F. Neese, *J. Chem. Theory Comput.*, 2008, **4**, 908–919.
39 H. Kruse and S. Grimme, *J. Chem. Phys.*, 2012, **136**, 154101.

40 J. G. Brandenburg, M. Alessio, B. Civalleri, M. F. Peintinger, T. Bredow and S. Grimme, *J. Phys. Chem. A*, 2013, **117**, 9282–9292.
41 A. Allouche, *J. Comput. Chem.*, 2011, **32**, 174–182.
42 P. A. Howell, R. M. Curtis and W. N. Lipscomb, *Acta Crystallogr.*, 1954, **7**, 498–503.
43 A. Chesney, M. R. Bryce, A. S. Batsanov and J. A. K. Howard, *Chem. Commun.*, 1997, 2293–2294.
44 I. Rowe and B. Post, *Acta Crystallogr.*, 1958, **11**, 372–374.
45 E. Meyers, K. Irgolic, R. Zingaro, T. Junk, R. Chakravorty, N. Dereu, K. French and G. Pappalardo, *Phosphorus, Sulfur Silicon Relat. Elem.*, 1988, **38**, 257–269.
46 A. Vashchenko, S. Kuznetsova and L. Somina, *J. Struct. Chem.*, 2012, **53**, 247–250.
47 S. Larson, S. Simonsen, G. Martin, K. Smith and S. Puig-Torres, *Acta Crystallogr., Sect. C: Cryst. Struct. Commun.*, 1984, **40**, 103–106.
48 K. Gallaher and S. Bauer, *J. Chem. Soc., Faraday Trans. 2*, 1975, **71**, 1173–1182.
49 P. Linstrom and W. Mallard, *National Institute of Standards and Technology*, *Gaithersburg MD*, 2005, 20899.
50 J. Beck, T. Bredow and R. T. Tjahjanto, *Z. Naturforsch.*, 2009, **64b**, 145.